# Improved tomographic imaging of wavelength scanning digital holographic microscopy by use of digital spectral shaping

**Lingfeng Yu and Zhongping Chen**

*Department of Biomedical Engineering, Beckman Laser Institute, University of California, Irvine, Irvine, CA 92612*
lingfeng@uci.edu, z2chen@uci.edu

**Abstract:** The technique of wavelength scanning digital holographic microscopy (WSDHM) is improved by use of a digital spectral shaping method which is used to suppress the sidelobes of the amplitude modulation function in WSDHM for non-Gaussian-shaped source spectra. Spurious structures caused by sidelobes can be eliminated in tomographic imaging and the performance of the tomographic system greatly improved. Detailed theoretical analysis is given. Both simulation and experimental results are presented to verify the idea.



**OCIS codes:** (090.1760) Computer holography; (110.0180) Microscopy; (110.6880) Three-dimensional image acquisition

## References and links

1. U. Schnars and W. Juptner, "Digital recording and numerical reconstruction of holograms," Meas. Sci. Technol. **13**, 85-101 (2002).
2. E. Cuche, F. Bevilacqua, and C. Depeursinge, "Digital holography for quantitative phase-contrast imaging," Opt. Lett. **24**, 291-3 (1999).
3. G. Indebetouw, "Properties of a scanning holographic microscope: improved resolution, extended depth-of-focus, and/or optical sectioning," J. Mod. Opt., **49**, 1479-1500 (2002).
4. E. Wolf, "Three-dimensional structure determination of semitransparent object from holographic data," Opt. Commun. **1**, 153–156 (1969).
5. W. H. Carter, "Computational reconstruction of scattering objects from holograms," J. Opt. Soc. Am. **60**, 306–314 (1970).
6. R. Dändliker and D. Weiss, "Reconstruction of three dimensional refractive index from scattered waves," Opt. Commun. **1**, 323–328 (1970).
7. A. F. Fercher, H. Bartelt, H. Becker, and E. Wiltschko, "Image formation by inversion of scattered field data: experiments and computational simulation," Appl. Opt. **18**, 2427–2439 (1979).
8. F. Charrière, A. Marian, F. Montfort, J. Kuehn, T. Colomb, E. Cuche, P. Marquet, and C. Depeursinge, "Cell refractive index tomography by digital holographic microscopy," Opt. Lett. **31**, 178-180 (2006)
9. M. K. Kim, "Tomographic three-dimensional imaging of a biological specimen using wavelength-scanning digital interference holography," Opt. Express **7**, 305–310 (2000).
10. M. K. Kim, L. Yu, and C. J. Mann, "Interference techniques in digital holography," J. Opt. A, Pure Appl. Opt. **8**, S518-S523 (2006).
11. L. Yu and M. K. Kim, "Wavelength-scanning digital interference holography for tomographic three-dimensional imaging by use of the angular spectrum method," Opt. Lett. **30**, 2092-2094 (2005)
12. L. Yu and M. K. Kim, "Wavelength scanning digital interference holography for variable tomographic scanning," Opt. Express. **13**, 5621–5627 (2005).
13. F. Montfort, T. Colomb, F. Charrière, J. Kühn, P. Marquet, E. Cuche, S. Herminjard, and C. Depeursinge, "Submicrometer optical tomography by multiple-wavelength digital holographic microscopy," Appl. Opt. **45**, 8209-8217 (2006)
14. D.Huang, E.A.Swanson, C.P.Lin, J.S.Schuman,W.G.Stinson, W.Chang, M.R.Hee, T.Flotte, K. Gregory, C.A.Puliafito, and J.G.Fujimoto, "Optical coherence tomography," Science **254**, 1178-1181 (1991).
15. W. Drexler, U. Morgner, F. X. Krtner, C. Pitris, S. A. Boppart, X. D. Li, E. P. Ippen, and J. G. Fujimoto, "Invivo ultrahigh-resolution optical coherence tomography," Opt. Lett. **24**, 1221-1223 (1999)
16. I. Hartl, X. D. Li, C. Chudoba, R. K. Ghanta, T. H. Ko, J. G. Fujimoto, J. K. Ranka, and R. S. Windeler, "Ultrahigh-resolution optical coherence tomography using continuum generation in an air silica microstructure optical fiber ," Opt. Lett. **26**, 608-610 (2001)

#77722 - $15.00 USD Received 4 December 2006; revised 11 January 2007; accepted 11 January 2007

17. Y. Zhang, M. Sato, and N. Tanno, "Resolution improvement in optical coherence tomography by optimal synthesis of light-emitting diodes ," Opt. Lett. **26**, 205-207 (2001)
18. R. Tripathi, N. Nassif, J. S. Nelson, B. H. Park, and J. F. de Boer, "Spectral shaping for non-Gaussian source spectra in optical coherence tomography," Opt. Lett. **27**, 406-408 (2002)
19. A F Fercher, W Drexler, C K Hitzenberger and T Lasser, "Optical coherence tomography - principles and applications," Rep. Prog. Phys. **66**, 239–303 (2003)
20. M. Alonso, and G. W. Forbes, "Measures of spread for periodic distributions and the associated uncertainty relations," Am. J. Phys. **69**, 340-347 (2001).

## 1. Introduction

Digital holography has become a subject of increasing interest for many researchers as it covers a great number of application areas, such as holographic interferometry for deformation or contour measurement, particle analysis, 3-D optical remote sensing, to name a few [1]. In digital holography, a CCD target is used for directly recording of a hologram which consists of an interference pattern produced by the reference and a three-dimensional (3D) object, and the wave field distribution and its propagation can be calculated by numerical algorithms in a computer. With digital holography, both the phase and intensity information of the reconstructed 3D field are readily available in numerical form and real-time processing of the image is possible, greatly simplifying metrological applications [2]. These advantages have stimulated the development of novel 3D microscopic techniques by using digital holography techniques. However, the reconstructed images from digital holography contain not only the information of the focused layer but also blurred information from the entire specimen. This out-of-focus blur has disastrous consequences when attempting to capture the three-dimensional structure of thick specimens or thick tissues [3].

In order to solve the above-mentioned problem in digital holographic 3D microscopic systems, the specimen needs to be scanned by changing the k vector of the illumination waves, according to the well-known optical diffraction tomography (ODT) theory [4-7]. One way to perform ODT with digital holography is to record holograms from different orientations of a rotating sample; then the three-dimensional refractive index spatial distribution of the sample can be reconstructed [8]. However, the forward detection requirement of the above scheme will normally limit its application in transparent or semi-transparent specimens. An alternative way to fulfill ODT is that the k vector is changed by scanning the wavelength of the illumination wave. This has been verified by the recently reported wavelength-scanning digital holographic microscopy (WSDHM) method [9-13]. The images are reconstructed from a number of holograms digitally recorded while the wavelengths are varied at regular intervals, and the numerical interference of the multiple three-dimensional hologram fields results in a synthesized short coherence length and corresponding narrow axial resolution which are inversely proportional to the span of the scanning wavelength. Variable tomographic scanning [12] made possible by reconstructing and superposing wavefields on tilted planes in space, and sub-micrometer axial resolution was reported [13] by increasing the wavelength scanning span to several hundred nanometers.

However, in all the previously reported WSDHM systems [9-13], the laser powers of all the scanning illumination wavelengths were adjusted to have the same weight, or the reconstructed wavefields from each wavelength were numerically normalized, so that the superposition of all the holographic fields resulted in a coherence depth-response envelope (or an amplitude modulation function as will be shown later). However, the above process has virtually resulted in a synthetic rectangular spectrum of the light source, which will cause big sidelobes in the amplitude modulation function. These sidelobes will actually generate severe spurious structures in tomographic imaging and will greatly increase the noise level of tomographic reconstruction. In this paper, we focus on the reduction of sidelobes in the coherence envelope and will propose a novel spectral shaping method to smooth out the sidelobes so that the performance of the digital holographic tomography system can be greatly improved.

#77722 - $15.00 USD Received 4 December 2006; revised 11 January 2007; accepted 11 January 2007

## 2. Principle

We will first briefly review the principle of wavelength scanning digital holographic microscopy [9-13]. A theoretical analysis of the method of digital spectral shaping will then be discussed. Suppose an object is illuminated by a laser beam of wavelength $\lambda$, any point *P* on the object at $\mathbf{r_P}$ scatters the incident beam into a Huygens wavelet $A(\mathbf{r_P})$, so that the resultant field $E(\mathbf{r})$ at $\mathbf{r}$ is

$$E(\mathbf{r}) \sim \int A(\mathbf{r_P}) \exp\left(ik|\mathbf{r}-\mathbf{r_P}|\right) d^3\mathbf{r_P}, \tag{1}$$

where *k* is the wave number and the integral is over the whole object volume. Now let us repeat the above holographic process using different wave numbers, and all the other conditions of the object or illumination are kept the same. If the reconstructed fields are all superposed together with infinite wave numbers, then the resultant field is

$$\begin{aligned} E(\mathbf{r}) &\sim \sum_k \int A(\mathbf{r}_\mathrm{P}) \exp\left(ik|\mathbf{r}-\mathbf{r_P}|\right) d^3\mathbf{r_P} \\ &\sim \int A(\mathbf{r}_\mathrm{P}) \sum_k \exp\left(ik|\mathbf{r}-\mathbf{r_P}|\right) d^3\mathbf{r_P} \\ &\sim \int A(\mathbf{r}_\mathrm{P}) M\left(|\mathbf{r}-\mathbf{r_P}|\right) d^3\mathbf{r_P} \\ &\sim A(\mathbf{r}), \end{aligned} \tag{2}$$

where $M\left(|\mathbf{r}-\mathbf{r_P}|\right) = \sum_k \exp\left(ik|\mathbf{r}-\mathbf{r_P}|\right)$ is defined as an amplitude modulation function (AMF) in this paper. As the number of wavelengths goes to infinite, the AMF actually become a delta function; thus, the resultant field is proportional to the field at the object and is nonzero only at the object points.

However, any physically existing light sources have a limited spectrum range of $[k_{\min}, k_{\max}]$, with a bandwidth of $\Delta k = k_{\max} - k_{\min}$. Practically, if one uses a finite number *N* of wave numbers at regular intervals of $dk = \frac{k_{\max} - k_{\min}}{N-1}$ from $[k_{\min}, k_{\max}]$, the above equation can be written as

$$\begin{aligned} E(\mathbf{r}) &\sim \int A(\mathbf{r}_\mathrm{P}) \sum_{k=k_{\min}}^{k_{\max}} \exp\left(ik|\mathbf{r}-\mathbf{r_P}|\right) d^3\mathbf{r_P} \\ &\sim \int A(\mathbf{r}_\mathrm{P}) \exp\left(i\bar{k}|\mathbf{r}-\mathbf{r_P}|\right) \frac{\sin\left(Ndk|\mathbf{r}-\mathbf{r_P}|/2\right)}{\sin\left(dk|\mathbf{r}-\mathbf{r_P}|/2\right)} d^3\mathbf{r_P}, \end{aligned} \tag{3}$$

where $\bar{k} = \frac{k_{\max} + k_{\min}}{2}$. Thus, except for an exponential term, the amplitude modulation function becomes

$$M\left(|\mathbf{r}-\mathbf{r_P}|\right) = \frac{\sin\left(Ndk|\mathbf{r}-\mathbf{r_P}|/2\right)}{\sin\left(dk|\mathbf{r}-\mathbf{r_P}|/2\right)}. \tag{4}$$

Clearly, the above process to obtain the amplitude modulation function is equivalent to the interference of a large number of monochromatic waves with equal intensities and equally spaced frequencies, which results in the generation of a narrow pulse of light. The amplitude modulation function has a periodic sequence of pulse-like peaks with a period (or beat wavelength) of $\Lambda = 2\pi[dk]^{-1}$ and the axial resolution $\delta = \Lambda/N = 2\pi/\Delta k$. Fig. 1 shows an example of an absolute AMF. Obviously, since the wavelength bandwidth of the light source is fixed, $\delta$ is always the same for different *N*. But the more wave numbers used, the bigger interval $\Lambda$ between the two peaks of the modulation function. Thus for tomographic imaging, other than the diffraction or defocusing effect of propagation, the reconstructed object image

#77722 - $15.00 USD Received 4 December 2006; revised 11 January 2007; accepted 11 January 2007

$A(\mathbf{r})$ will also repeat itself at a beat wavelength $\Lambda$ with axial resolution of $\delta$. By using appropriate values of *dk* and *N*, the beat wavelength $\Lambda$ can be matched to the axial extent of the object and $\delta$ to the desired level of axial resolution.

At the extreme, if all the wave numbers within the bandwidth $[k_{\min}, k_{\max}]$ are continuously scanned for illumination and reconstruction, it can be easily shown that the normalized amplitude modulation function finally become a sinc function as

$$\bar{M}\left(|\mathbf{r}-\mathbf{r_P}|\right)=\frac{\sin\left(\Delta k|\mathbf{r}-\mathbf{r_P}|/2\right)}{\Delta k|\mathbf{r}-\mathbf{r_P}|/2}. \tag{5}$$

Thus, the beat wavelength $\Lambda$ will become infinitely large, and the axial resolution remains the same as in Eq. (4).

From the above equations, it is noticed that the amplitude modulation function actually forms a Fourier transform pair with the spectral shape of the light source as in optical coherence tomography [14]. Because **r** and k space form a Fourier transform pair, equally k-spaced wavelengths are always preferred for scanning. A tunable laser is normally used as a light source which is sequentially scanned to obtain the equally k-spaced wavelengths. Each wavelength corresponds to a quasi-Dirac spectrum (very narrow compared to the tuning range) of the source. However, all previously reported WSDHM systems gave these different wavelengths the same weight, or the reconstructed wavefields from each wavelength were numerically normalized. This resulted in a synthetic rectangular or limited-sampled-rectangular shape spectra of the light source; thus either the AMF from Eq.(4) or Eq.(5) will cause big sidelobes which are not well suppressed. These sidelobes will generate severe spurious structures in tomographic imaging and increase the average noise level of the reconstruction.

In order to solve these problems, the concept of spectral shaping is introduced to the WSDHM system in this paper. Spectral filtering [15,16] and shaping [17] were previously reported to obtain Gaussian spectra from non-Gaussian sources in order to improve the point-spread function in optical coherence tomography. Similarly, in WSDHM, because of the Fourier transform relationship between the AMF and light source spectra, it follows the Fourier uncertainty relation that Fourier transform of a Gaussian function is another Gaussian, and the product of variances of Fourier transform pairs reach minimum for Gaussian functions [19]. Thus, digitally correcting the non-Gaussian spectra could result in the reduction of sidelobes in the amplitude modulation function and eliminate spurious structures in tomographic imaging. This paper proposes and demonstrates a weighing method of each wavelength wavefront in order to "simulate" a wide Gaussian spectrum source.

Assume that the light source power spectrum is finally shaped to a Gaussian spectral form:

$$S(k-\bar{k})=\frac{1}{\sqrt{2\pi}\sigma_k}\exp\left[-\frac{\left(k-\bar{k}\right)^2}{2\sigma_k^2}\right], \tag{6}$$

which has been normalized to unit power,

$$\int_{-\infty}^{\infty} S(k-\bar{k})dk=1, \tag{7}$$

where $\bar{k}$ is the center wave number and $2\sigma_k$ is the standard deviation power spectral bandwidth.

The resultant wavefield in Eq.(2) can then be written as

$$\begin{aligned} E(\mathbf{r}) &\sim \int_k S(k-\bar{k})\int A(\mathbf{r}_P)\exp\left(ik|\mathbf{r}-\mathbf{r_P}|\right)d^3\mathbf{r_P}\cdot dk \\ &\sim \int A(\mathbf{r}_P)\int_k S(k-\bar{k})\exp\left(ik|\mathbf{r}-\mathbf{r_P}|\right)dk\cdot d^3\mathbf{r_P}. \end{aligned} \tag{8}$$

#77722 - $15.00 USD Received 4 December 2006; revised 11 January 2007; accepted 11 January 2007

Obviously, the amplitude modulation function $M\left(\left|\mathbf{r}-\mathbf{r_P}\right|\right)$ now becomes the Fourier transform of the Gaussian spectra $S(k-\bar{k})$. Thus, the amplitude modulation function contains a Gaussian envelope as well with a characteristic standard deviation spatial width $2\sigma_x$ that is inversely proportional to the power spectral bandwidth, which means that $\sigma_x\sigma_k=1$. This is the limiting case of a general inequality on the product of variances of Fourier transform pairs. In general, if *S* is an arbitrary distribution and *M* is its Fourier transform, then the product of the variations is greater than one. This confirms the Fourier uncertainty relation that the product of variances of a Fourier transform pair reaches its minimum for Gaussian functions. If the above product is not minimized, then the AMF must not be a Gaussian. In this paper, a final Gaussian shape is always aimed by spectral shaping. In numerical implementation, an *N*-point Gaussian spectra covering the spectrum range of $[k_1,k_N]$ is obtained by digitizing Eq. (6) as

$$S(n+1)=\exp\left[-\frac{1}{2}\left(\alpha\frac{k_1+ndk-\bar{k}}{(k_N-k_1)/2}\right)^2\right], \tag{9}$$

where $0\le n\le N-1$, and $\alpha$ is a parameter introduced to adjust the width of the Gaussian spectra. We have ignored the constant before the exponential term in Eq.(6). The influence of the parameter $\alpha$ on spectral shaping will be studied below.

### 3. Simulations and Experiments

Both numerical simulations and experiments were carried out to verify the effectiveness of the proposed idea. Since amplitude is of more concern in tomographic imaging, we only plotted the absolute amplitude modulation functions. Fig. 1. shows several absolute AMFs when different numbers of equally k-spaced wavelengths between 1260nm and 1340nm were used for WSDHM. The light powers for each wavelength were assumed to be the same. In this case, the AMF was expressed as Eq. (4) and had a periodic sequence of pulse-like peaks with period $\Lambda=2\pi[dk]^{-1}$ and axial resolution $\delta=\Lambda/N$. The more wavelengths used, the bigger beat wavelength $\Lambda$, but the axial resolution $\delta$ did not change. For example, Fig. 1(a) shows the amplitude modulation function when 25 wave numbers were used for tomographic imaging which resulted in the beat wavelength $\Lambda=506.5\mu m$ and axial resolution $\delta=21.1\mu m$. A total axial range from -600 $\mu m$ to 600 $\mu m$ was covered in Fig. 1., and three peaks appear in Fig. 1(a). As 50 wave numbers were used, the beat wavelength changed to $\Lambda=1034.1\mu m$ but the axial resolution $\delta$ was unchanged, as indicated in Fig. 1(b) where the mainlobe width at -3dB was about 24.96 $\mu m$. At the extreme, as the number *N* went to infinity so that a continuous spectra range was considered, the AMF finally became a sinc function as Eq.(5) and is shown in Fig. 1(c), The mainlobe width at -3dB in this case was about 25.44 $\mu m$, which is almost the same as in Fig.1(b). Note that the sidelobes of all the above AMF are not well suppressed. For example, the first order sidelobe in either Fig. 1(b) or 1(c) reaches about 21.8% of the main peak amplitude, which corresponds to a -13.2 dB sidelobe attenuation in decibels. Clearly, the non-suppressed sidelobes introduce severe artifacts (or spurious structures) in reconstruction. Although it might be possible to use deconvolution methods to partially correct these sidelobe effects, it is hard to completely remove these effects because of the existence of phase and amplitude noise in real images. These artifacts are not true noise, but they act as “background noise” on the reconstructed image planes, if we consider any information excepting the “real signal” as a “noise.” In this sense, the authors are using the term “noise” in the paper. We can find that the average background noise becomes larger because of the existence of these non-suppressed sidelobes.

#77722 - $15.00 USD Received 4 December 2006; revised 11 January 2007; accepted 11 January 2007

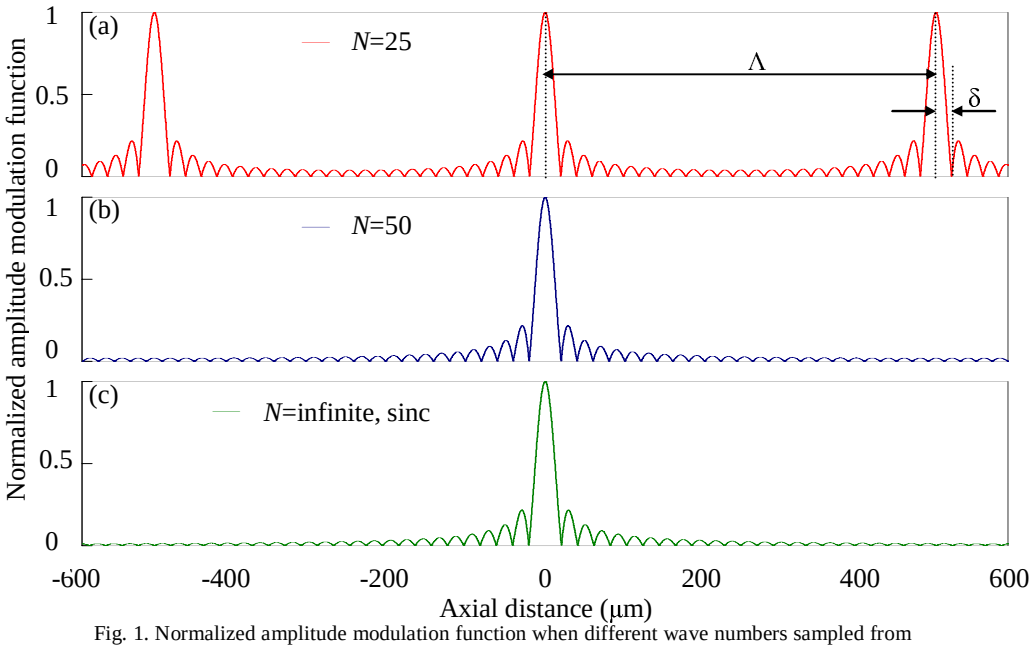


Fig. 1. Normalized amplitude modulation function when different wave numbers sampled from 1260nm to 1340nm are used for tomographic imaging with (a) $N$=25; (b) $N$=50; and (c) continuously sampled wave numbers.

The sidelobes of AMF in WSDHM could be greatly suppressed by Gaussian spectral shaping. Fig. 2(a) shows the amplitude modulation function with Gaussian spectral shaping ($\alpha = 2.5$) when 50 wave numbers are used for reconstruction. For comparison, the amplitude modulation function without Gaussian spectral shaping is also plotted in the Fig.. Fig. 2(b) shows the same AMFs in decibel scale. One can see that the relative sidelobe attenuation now becomes -43.2dB, which is greatly improved compared to Fig. 1. And there is about 20dB attenuation of the average noise level by use of Gaussian spectral shaping. The mainlobe width at -3dB is about 39.7 $\mu m$ which can now be considered as the axis resolution of the WSDHM system.

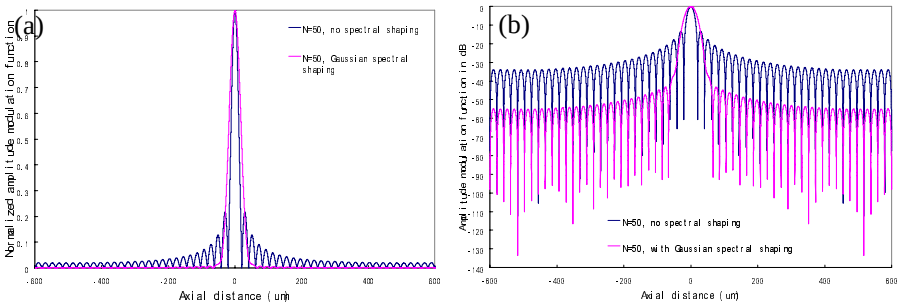


Fig. 2. Amplitude modulation function with and without Gaussian spectral shaping when 50 wave numbers are scanned from 1260nm to 1340nm; plotted in (a) linear and (b) decibel scale.

The effect of the parameter $\alpha$ on spectral shaping is also studied. Fig. 3 shows the amplitude modulation function in linear and decibel scales when different values of $\alpha$ are used in Eq.(9) for Gaussian spectral shaping. According to the property of Gaussian function, the width of the Gaussian envelope is inversely proportional to the value of $\alpha$ : a bigger value of $\alpha$ ($\alpha \geq 2$) induces a more narrow spectra but a broader AMF. A smaller $\alpha$ ($\alpha < 2$), however, will cut a portion of a broader Gaussian envelope; thus, sidelobes will appear in AMF, as shown in Fig. 3. Therefore, $\alpha \geq 2$ is preferred in our application.

#77722 - $15.00 USD Received 4 December 2006; revised 11 January 2007; accepted 11 January 2007

Note that the mainlobe width after Gaussian spectral shaping is bigger before shaping in Fig. 2. This is because the spectral shaping operation actually narrows down the effective width of the synthetic rectangular spectra and results in a bigger axial resolution. So there is a trade-off between the side-lobe suppression and the axial resolution of the system, which can be adjusted by the parameter α. As one can see from Fig. 3, a value of $\alpha = 2.5$ will normally guarantee both a good axial resolution and well-suppressed sidelobes in AMF. We will use this value for spectral shaping in the following section.

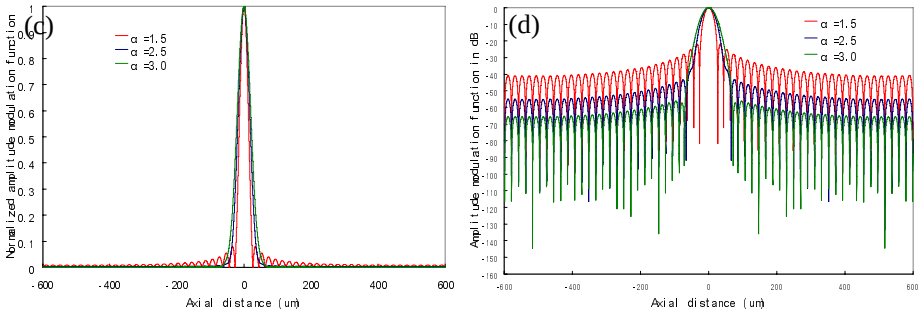


Fig. 3. Different α for Gaussian spectral shaping when 50 wave numbers are scanned from 1260nm to 1340nm; plotted in (a) linear and (b) decibel scale.

Experiments were also performed to verify the proposed idea using the apparatus depicted in Fig. 4. A Santec TSL-210V laser was scanned continuously from 1260 nm to 1340 nm to obtain a sequence of equally k-spaced wavelengths, with a constant 10mw optical output for each wavelength. The laser output was collimated and split into reference and object beams in an interferometer based on the Michelson configuration. The object specimen was placed at a distance z from the hologram plane S, whose magnified image was projected on an InGaAs camera (Sensors Unlimited SU640) as well as the reference beam. A slight angle was introduced between the object and the reference beams by tilting the reference mirror REF for off-axis holography. An aperture was placed in the focal plane of L2 (a low NA achromatic doublet from Thorlabs, AC254-075-C) to control the size of the object spectrum captured in the camera which had an array of 640 × 512 pixels with a 25 $\mu m$ pitch size and 12-bit gray scale output. A camera link cable connected the camera to the desktop computer which processed the acquired images and calculated the holographic diffraction using a number of programs based on LabVIEW® and MatLab®.

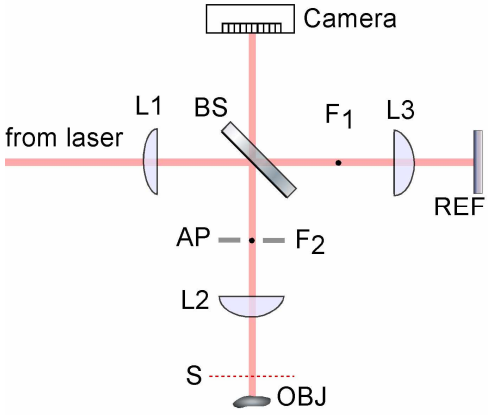


Fig. 4. Optical apparatus used in the digital holographic microscopy experiments. The Ls are various lenses; BS is a beamsplitter; AP is an aperture and REF is a mirror. F1 or F2 are focal points of lens L1, and Point F2 is also the back focus of L2. The CCD camera captures the image of the interference pattern at the plane S.

#77722 - $15.00 USD Received 4 December 2006; revised 11 January 2007; accepted 11 January 2007

In order to demonstrate the idea, a selected area on a USAF 1951 resolution target, with 2.4×2.4 $mm^2$, 256×256 pixels, was observed by the WSDHM system. There are two ways to perform reconstruction. If we consider the reconstruction in the "image domain," then the CCD camera records the hologram, and we use the distance between the image plane (image of the object through L2) and the CCD plane for reconstruction. Alternatively, we could also consider the reconstruction in the "object domain." In this case, the image of the CCD plane (S plane) records a hologram of the object, then the distance between the S plane and the object plane is directly used for reconstruction. We are using the latter way for reconstruction. The reconstruction distance z, representing the distance from the object to S plane in Fig. 4 was about 3mm. A series of holograms were recorded using 50 equally separated wave numbers. As has been discussed above, this gave a beat wavelength of 1034.1 μm. The image volume was calculated from each of the holograms by use of numerical algorithms in the computer and all such image volumes were numerically superposed to create the 3D tomographic image [11,12].

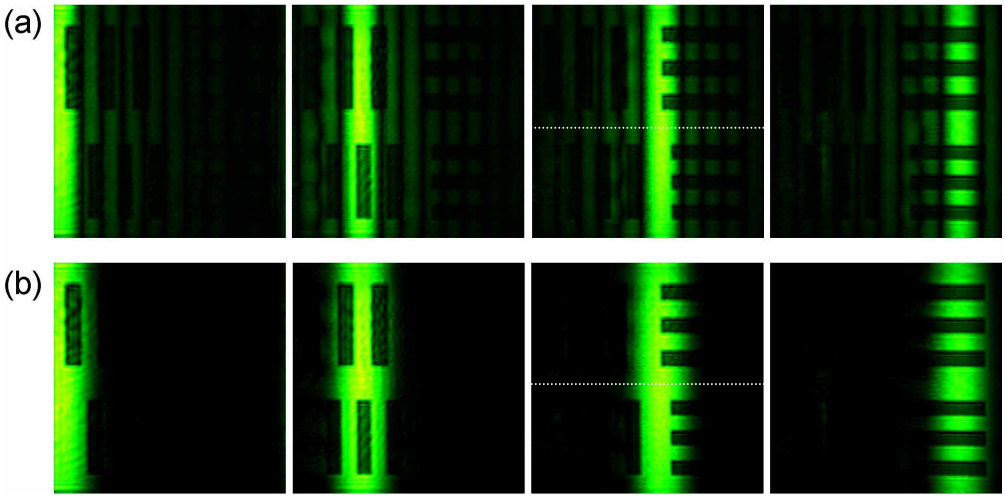


Fig. 5. A sequence of contour images at different layers: (a) without; and (b) with Gaussian spectral shaping.

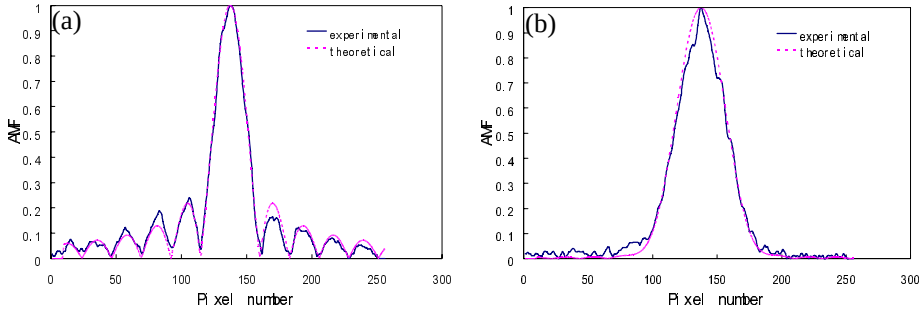


Fig. 6. Comparison of the experimentally obtained AMF with its theoretical value: (a) without and (b) with Gaussian spectral shaping.

Figure 5(a) shows a sequence of tomographic images reconstructed without Gaussian spectral shaping. Since the target was slightly tilted relative to the hologram plane, the contour images sequentially appear from left to right in Fig. 4 as the distance z is increased. The AMF of the system was experimentally measured by sampling a labeled cross line of a tomographic image in Fig. 5(a) and is plotted in Fig. 6(a), which also shows the theoretical AMF for comparison. One can clearly see the unsuppressed sidelobes in these Fig.s, and the experimental AMF agrees well with its theoretical value. Obviously, Fig. 5(a) provides

#77722 - $15.00 USD Received 4 December 2006; revised 11 January 2007; accepted 11 January 2007

spurious structure information for the resolution target since it is known that the resolution target has a clear pattern on a flat chrome background. The results with Gaussian spectral shaping in WSDHM are shown in Fig.5(b) where we have used $\alpha = 2.5$ in Eq. (9) to guarantee both a good axial resolution and well suppressed sidelobes in AMF. The experimental AMF from a cross line is also shown in Fig. 6(b), and it fits well with its theoretical prediction. Clearly, the sidelobes have now been greatly suppressed in AMF. If we consider the spurious ripples as background noise and analyze the experimental AMFs of both the above cases in decibel scale, it shows that there is about 15 dB improvement in the average noise level, which results in a signal-to-noise ratio gain by using Gaussian spectral shaping.

To further demonstrate the concept, we consider a 3D example previously reported in Ref. 11. A penny with an area of 2.62 mm×2.62 mm was illuminated by a dye laser scanning from 575.0 nm to 605.0 nm with 20 equally k-spaced steps. The contour images reconstructed without Gaussian spectral shaping are shown in Fig. 7(a) [11]. The sidelobe effects are clearly seen in these images. For comparison, Fig. 7(b) shows the result when the proposed method of Gaussian spectral shaping is used for reconstruction from the same data set. The suppression of sidelobes by using Gaussian spectral shaping is evident.

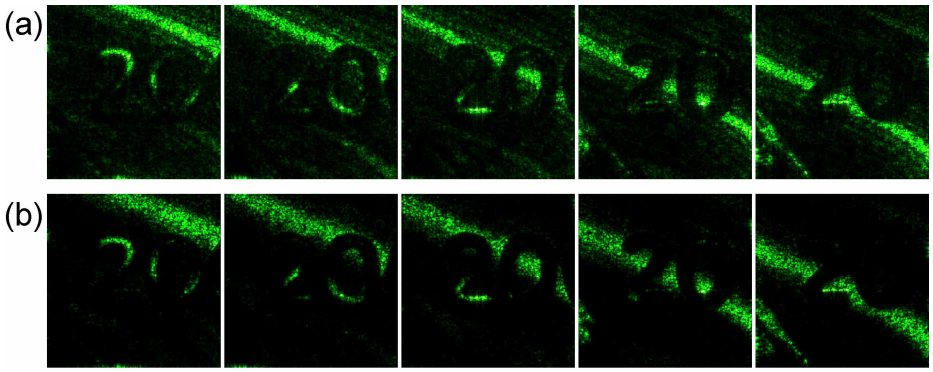


Fig. 7. Several contour images of the coin reconstructed (a) without [11] and (b) with Gaussian spectral shaping.

## 4. Conclusion

In conclusion, Gaussian spectral shaping can be successfully applied to suppress the sidelobes in the amplitude modulation function of WSDHM, so that not only the average noise level in reconstruction is decreased, the signal-to-noise ratio of the system improved, but spurious structures in tomographic imaging eliminated. The proposed method could be used to greatly improve the performance of a WSDHM system. Although the examples presented only show the surface profiles of simple objects, the capability of WSDHM to generate cross-sectional views of sub-surface biological structures has been experimentally demonstrated elsewhere [9-10].

This work was supported by research grants from the National Institutes of Health (EB-00293, NCI-91717, and RR-01192), Air Force Office of Scientific Research (FA9550-04-1-0101), and the Beckman Laser Institute Endowment.

#77722 - $15.00 USD Received 4 December 2006; revised 11 January 2007; accepted 11 January 2007